Control of the CET Localization in Continuously Cast Copper and Copper Alloys' Ingots

P. Kwapisiński [a], *, **W. Wołczyński** [b]

[a] KGHM Polska Miedź S.A., M. Skłodowskiej-Curie 48, 59-301 Lubin, Poland
[b] Institute of Metallurgy and Materials Science, W. Reymonta 25, 30-059 Kraków, Poland
* Corresponding author E-mail address: Piotr.Kwapisinski@kghm.com

Abstract

A brief description of the innovative mathematical method for the prediction of *CET* – localization in solidifying copper and copper alloys' ingots is presented. The method is to be preceded by the numerical simulation of both temperature field and thermal gradient filed. All typical structural zones were revealed within the copper and copper alloys' massive ingots or rods manufactured by continuous casting. The role of thermal gradient direction for the single crystal core formation has been enlightened. The definition for the index describing proportion between volume fraction of the columnar structure and volume fraction of the equiaxed structure has been formulated by means of the interpretation of some features of the liquidus isotherm velocity course. An attempt has been undertaken to apply the developed mathematical method for the structural zones prediction in the rods solidifying under industrial conditions. An industrial application has been shown, that is, it was explained why the innovative rods should be assigned to the overhead conductors in the electric tractions.

Keywords: Proportion index for cellular / equiaxed fraction, Liquidus isotherm velocity, Single crystal's core, Structural zones

1. Introduction

Continuously cast copper and copper alloys' ingots were manufactured in the KGHM Polska Miedź S.A. and its business partners such as Non-Ferrous Metals Rolling Mill "Łabędy" or Metal Rolling Mill "Dziedzice" S.A.. Recently, the Copper Smelter "Cedynia" has delivered the Cu-Ag rods manufactured by the *Upcast* – technology.

According to the solidification rules, at first, the columnar structure shell is formed in an ingot, [1]. It precedes the equiaxed structure growth from the undercooled liquid, [2].

Thus, the T – structural transition from the C – columnar structure into the E – equiaxed structure, *CET*, is to be usually observed in such products like: strands, ingots or rods.

The mentioned transition is the result of the conversion of the solidification conditions which are responsible for constrained growth into solidification conditions which trigger unconstrained free growth during the process under investigation, [3].

The *CET* can occur immediately and it is sharp transition or can be observed in time and it is progressive transition, [4].

Some numerical treatments made attempts to reproduce a localization of the *CET* revealed within the samples or directly in the ingots manufactured under industry conditions, [2].

Usually, the temperature field was calculated to show the situation of both liquidus isotherm and solidus isotherm. It allowed to define the mushy zone within a solidifying ingot, as well as to conclude where the *CET* could appear, [5-14].

Similar simulations were performed for some samples subjected to solidification under microgravity, [15-20].

2. Revealing of *CET* within the copper and copper alloys' ingots / strands

Many copper and copper alloys' ingots / strands were cut to reveal the appearance of the *CET* – phenomenon within the slices, Fig. 1.
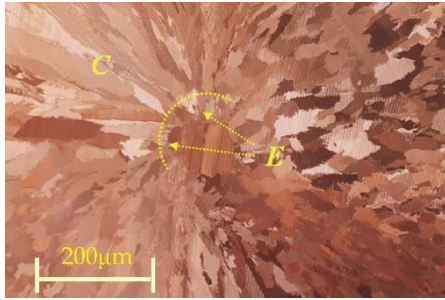

Fig. 1a. Selected area of the slice cut from the oxygen-free copper ingot; sharp *CET* marked; visible single crystal situated axially; ingot diameter: 295 mm; pulling rate of the ingot: 90 mm/min.
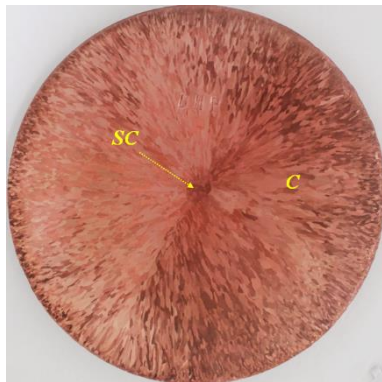

Fig. 1b. Phosphorous cooper slice / ingot; no *CET* revealed; SC visible; ingot diameter: 295 mm; pulling rate: 130 mm/min.
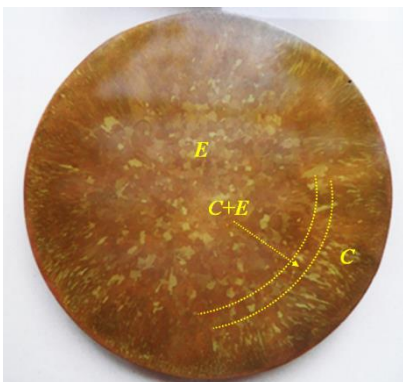

Fig. 1c. Cu-37Zn brass slice / ingot; progressive *CET* revealed; ingot diameter: 240 mm: pulling rate: 100 mm/min., [21]

Fig. 1d. Cu-0.1Ag strand 60mm x 120 mm in the cross-section; *Contirod* – technology; *C* – structure revealed, exclusively.
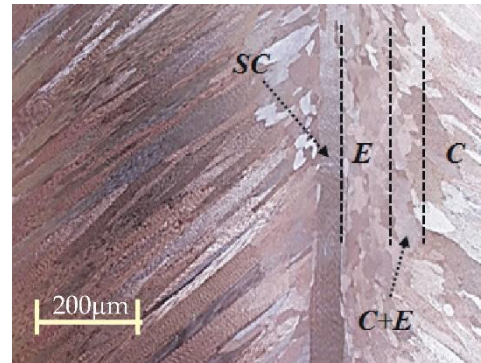

Fig. 1e. Longitudinal section of the oxygen-free copper ingot; progressive *CET* revealed, *SC* – single crystal situated axially; ingot diameter: 270 mm; pulling rate: 90 mm/min., [22]
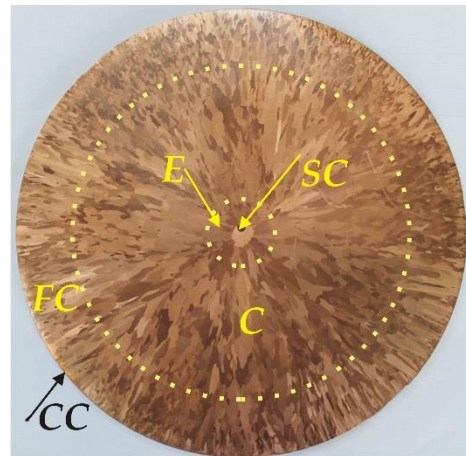

Fig. 1f. Oxygen-free copper slice / ingot; $CC \Rightarrow FC$, $FC \Rightarrow C$, $C \Rightarrow E$, and $E \Rightarrow SC$ sharp transitions revealed; ingot diameter: 270 mm; pulling rate: 130 mm/min.

The above shown morphologies present the following types of the ingots' structure: *C* – columnar, *E* – equiaxed, *CC* – chilled columnar, *FC* – fine columnar, and *SC* – single crystal situated axially.

The *CET* was revealed in major number of ingots, Fig. 1a, Fig. 1c, Fig. 1e, and Fig. 1f. However, the progressive *CET* is visible in the case of the ingots shown in Fig. 1c, and Fig. 1e.

The existence of the *C+E* – zone is characteristic for the progressive *CET* occurrence.

3. Results of numerical simulation

Some numerical simulations for heat transfer during continuously cast Cu-5Zn ingot have been performed. The heat transfer equations were formulated within the co-ordinate system attached to the s/l interface, [23]. Thus, the co-ordinate system was walking during simulation with the velocity similar to the pulling rate of the ingot through the crystallizer.

The achieved temperature field has been transformed into the thermal gradient field to allow for analysing some functions and maps which yield from both fields. First of all, a map illustrating the mushy zone location can be shown when the gap between the ingot and crystallizer surface is subjected to an adjusting, Fig. 2.
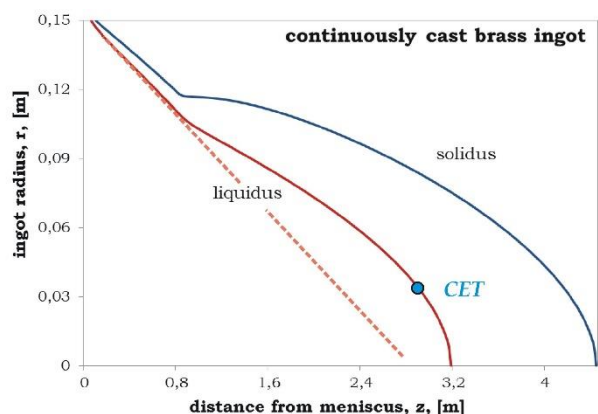

Fig. 2a. Location of the mushy zone for the gap: $\delta = 0.0117$ mm; alloy composition: Cu-40Zn, ingot diameter: 30 cm, pulling rate: 40 cm/min., crystallizer height: 80 cm
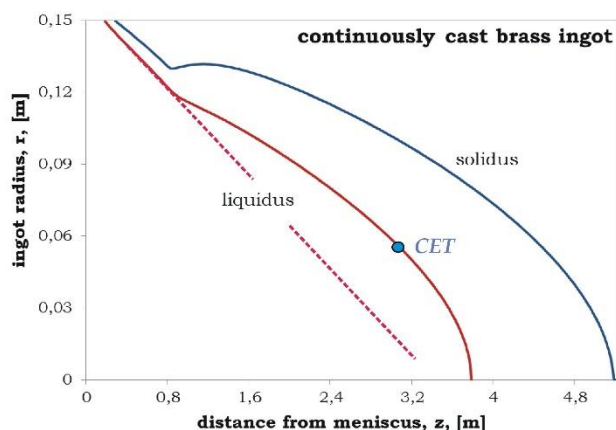

Fig. 2b. Location of the mushy zone for the gap: $\delta = 0.0234$ mm; alloy composition: Cu-40Zn, ingot diameter: 30 cm, pulling rate: 40 cm/min., crystallizer height: 80 cm

The location of the mushy zone is very sensitive on the thickness of gap resulting from the ingot's shrinkage as it is shown in Fig. 2.

Thus, the conclusion can be formulated that location of the mushy zone and resulting possible situation of the *CET* can be substantially controlled by the gap thickness setting.

The crystallizer height applied to the performed simulation was equal to: $H = 80$ cm. Therefore, the characteristic cusps of the liquidus and solidus isotherms' course / situation are visible in the discussed maps, just at a proper distance from meniscus, Fig. 2.

The performed simulations allowed for analysing the effect of a given pulling rate through crystallizer: $u = 90$ cm/min., Fig. 3, and $u = 250$ cm/min., Fig. 4, on the precise location of *CET*.
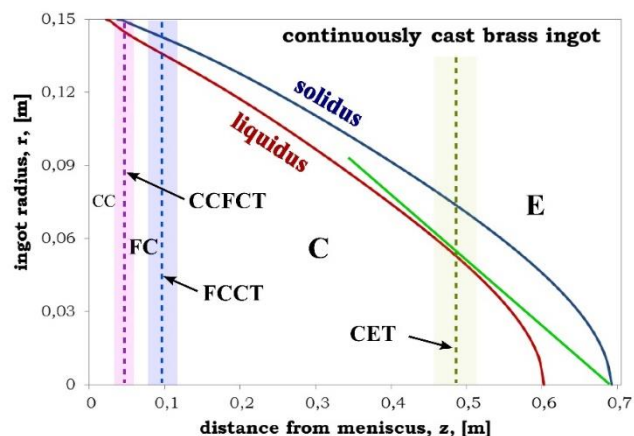

Fig. 3a. *CET* location in $r(z)$ - map as determined by maximum deviation from virtual linear course of the liquidus isotherm; alloy composition: Cu-5Zn, ingot diameter: 30 cm, ingot height: 200 cm, pulling rate: 90 cm/min., crystallizer height: 80 cm

Fig. 3b. *CET* location in $r(t)$ - map as determined by maximum deviation from virtual linear course of the liquidus isotherm; alloy composition: Cu-5Zn, ingot diameter: 30 cm, ingot height: 200 cm, pulling rate: 90 cm/min., crystallizer height: 80 cm

The *CET* localization was determined by the tangent (green line) to the course of liquidus isotherm. The *CET* determination is shown schematically without precise calculation of the first derivative related to mathematical function describing the course of liquidus isotherm. The virtual linear course of the liquidus isotherm is thought as the extension of its initial linear situation resulting from calculation.

Fig. 3c. *CET* location in the $\partial T / \partial r(z)$ - map as determined by the inflection point of the liquidus isotherm; alloy composition: Cu-5Zn, ingot diameter: 30 cm, ingot height: 200 cm, pulling rate: 90 cm/min., crystallizer height: 80 cm
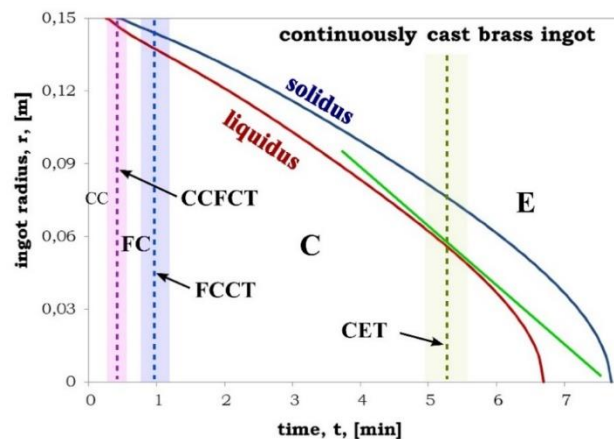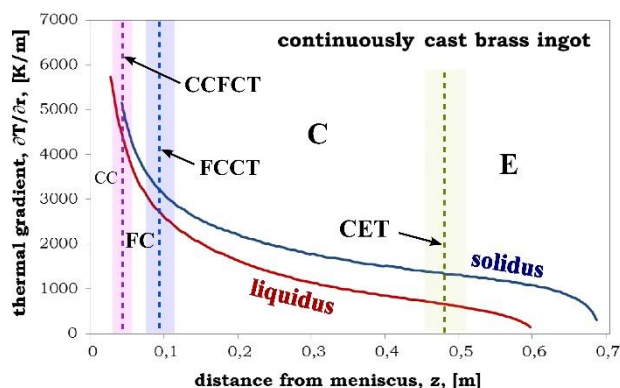

Fig. 4a. *CET* location in $r(z)$ - map as determined by maximum deviation from virtual linear course of the liquidus isotherm; alloy composition: Cu-5Zn, ingot diameter: 30 cm, ingot height: 200 cm, pulling rate: 250 cm/min., crystallizer height: 80 cm

It is to be emphasized that the localization of *CET* is similar, in first approximation, while considering the $r(z)$ - map, Fig. 3a and the $\partial T / \partial r(z)$ - map, Fig. 3c.

This localization is equal to about 48 cm from the meniscus in both situations, Fig. 3a, Fig. 3c. It means that *CET* occurs inside the crystallizer which has its height equal to 80 cm.

The similar result was obtained in the case of application of the higher pulling rate, Fig. 4a, Fig. 4c. Then, *CET* is localized about 150 cm from the meniscus, Fig. 4a, Fig. 4c.

However, *CET* occurs beyond the crystallizer which has the same height equal to 80 cm, and a typical cusp of the liquidus isotherm appears a little after the crystallizer edge, Fig. 4.

CET is observed just after 5 minutes of the process duration while applying the pulling rate equal to 90 cm/min., Fig. 3b, and a little after 6 minutes of the process duration while applying the pulling rate equal to 250 cm/min., Fig. 4b.
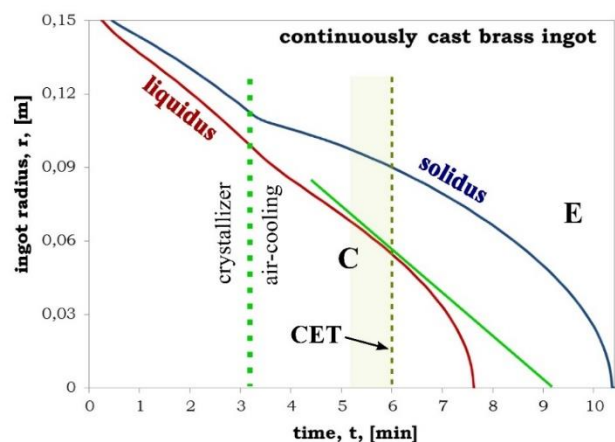

Fig. 4b. *CET* location in $r(t)$ - map as determined by maximum deviation from virtual linear course of the liquidus isotherm; alloy composition: Cu-5Zn, ingot diameter: 30 cm, ingot height: 200 cm, pulling rate: 250 cm/min., crystallizer height: 80 cm
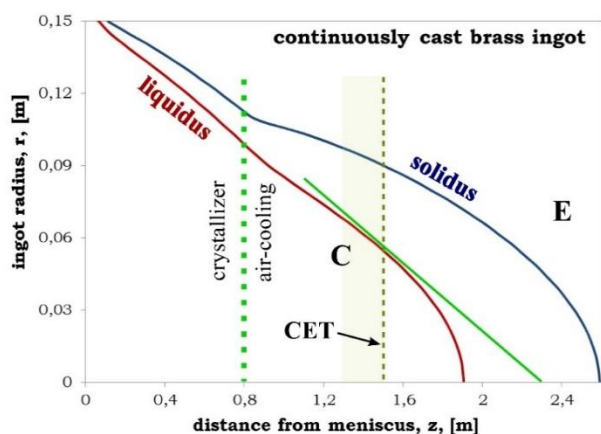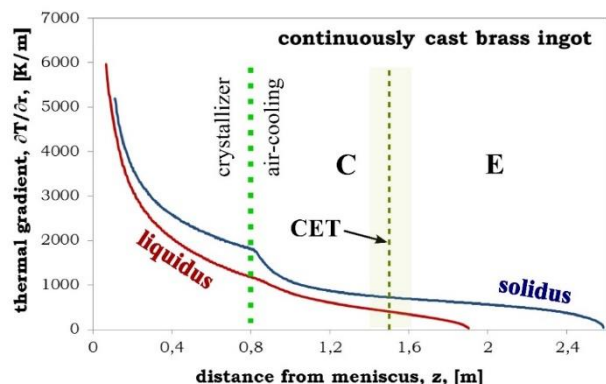

Fig. 4c. *CET* location in the $\partial T / \partial r(z)$ - map as determined by the inflection point of the liquidus isotherm; alloy composition: Cu-5Zn, ingot diameter: 30 cm, ingot height: 200 cm, pulling rate: 250 cm/min., crystallizer height: 80 cm

4. Role of thermal gradient direction in the ingot's structure formation

Thermal gradient G_C is directed along the columnar grains axis during solidification. However, its radial component was subjected to consideration in the performed simulation, Fig. 3c, Fig. 4c.

It seems that this radial component $G_r = \partial T / \partial r$ plays an essential role while the equiaxed structure is growing. However, thermal gradient is subjected to a substantial rotation when the single crystal's core appears along the ingot axis, Fig. 1a, Fig. 1b, Fig. 1e, Fig. 1f. In this case, thermal gradient becomes directed vertically. Therefore, it is denoted as the G_z - gradient.

The mentioned rotation of the thermal gradient direction can be well illustrated in a longitudinal section of the ingot or rod manufactured by the continuous casting. Fig. 5.
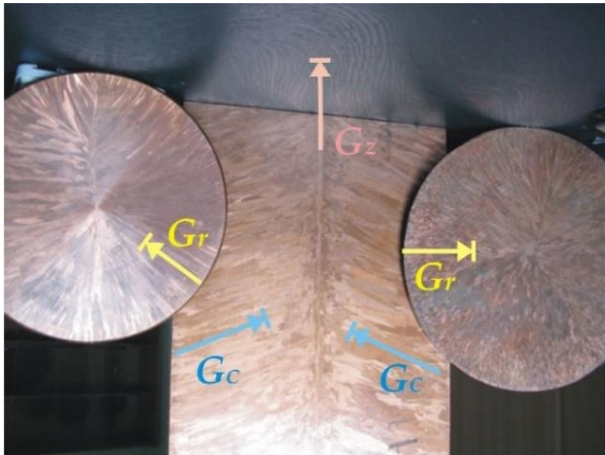

Fig. 5a. Virtual localization of the thermal gradients during the ingots solidification according to a continuous casting downward; visible revealed structures: C – columnar, E – equiaxed, and SC – single crystal situated axially
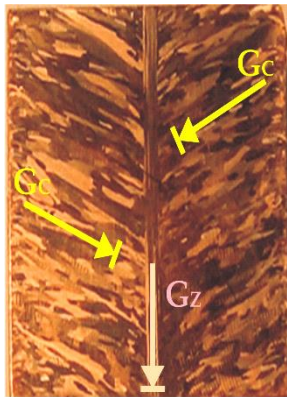

Fig. 5b. Virtual localization of the thermal gradients during the rod solidification according to a continuous casting upward, *Upcast* - technology, revealed structures: C – columnar, and SC – single crystal situated axially

5. Index of columnar / equiaxed grains' proportion

On the basis of some pole figures measurement, it has been proven that the columnar structure do not easily yield to plastic deformation, whereas the equiaxed structure evinces many slip systems, which is favorable for the mentioned deformation, [24].

Hence, it is very important for the plastic deformation requirements to create a fraction of the equiaxed structure as substantial as possible, and simultaneously a minor fraction of the columnar structure. The latter one can be accompanied by a single crystal positioned axially, Fig 1a, Fig. 1b, Fig. 1e, Fig. 1f, Fig. 5.

Therefore, the index defining a proportion between the fraction of the columnar structure and the fraction of the equiaxed structure is to be formulated.

The required definition has been developed on the basis of the interpretation of the liquidus isotherm velocity course along the mushy zone, Fig. 6.
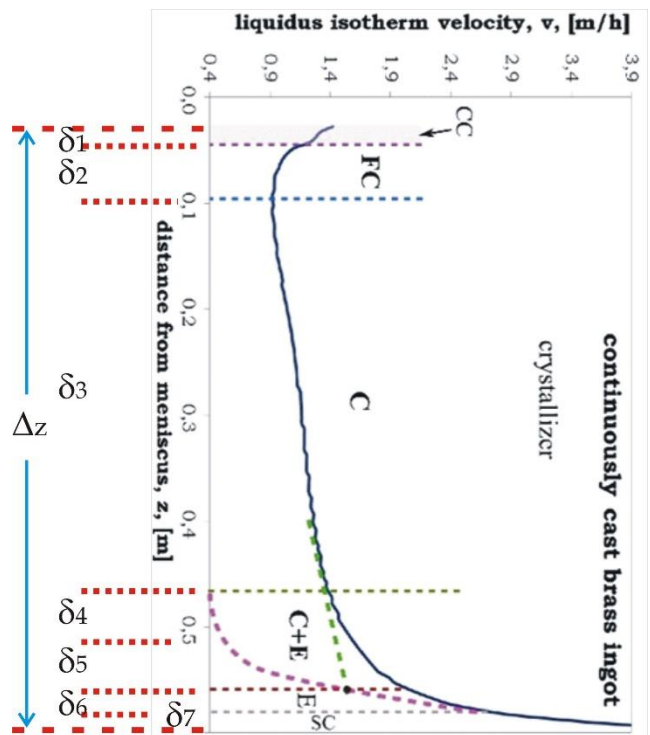

Fig. 6. *Structure formation ranges*, δ_i, along the mushy zone, Δz; alloy composition: Cu-5Zn, ingot diameter: 30 cm, pulling rate: 90 cm/min., crystallizer height: 160 cm, gap thickness a little corrected in comparison with $\delta = 0.0234$ mm (a little lower)

Some transitions between *structural zones* selected in the slice cut from an ingot, Fig. 1f, are reproduced as *structure formation ranges* while subjecting the liquidus isotherm velocity course, achieved for similar ingot, Fig. 6, to mathematical interpretation.

Hence, $CC \Rightarrow FC$ appears at the cusp of the liquidus isotherm velocity, $FC \Rightarrow C$ is located just at the beginning of linear course, $C \Rightarrow E$ presents the progressive character, thus, it is accompanied by the $C+E$ zone formation at the completion of linear course, the E – structure formation begins at the intersection of two (dashed) lines resulting from extension of both linear courses, $E \Rightarrow SC$ is sharp transition and locates at the beginning of the second linear course of the function under consideration, Fig. 6.

The following definition for determining the location of *structural zones* along the ingot's radius has been formulated:

$$\psi_i = \left(\delta_i / \Delta z \right) \cdot \Theta, \qquad i = 1,...,7 \qquad (1)$$

where, $i = 1,...,7 \equiv CC, FC, C, C+E, E+C, E, SC$, Fig. 6, and Θ is a given ingot radius.

Thus, the p_K - index defining proportion between volume fractions of columnar and equiaxed structures is written as:

$$p_K = \frac{\Theta^2 - \left[\Theta - \left(\psi_{CC} + \psi_{FC} + \psi_C + \psi_{CE}\right)\right]^2 + \psi_{SC}^2}{\left(\psi_{EC} + \psi_E + \psi_{SC}\right)^2 - \psi_{SC}^2} \qquad (2)$$

The p_K - proportion index is an effective tool in controlling the CET localization since this structural transition seems to be fundamental while considering some needs of the foundry engineering, [25], [26], [27].

6. Structural zones' control - industrial application of the mathematical method

The current mathematical method used for the reproduction of the *structural ranges formation* analyses some features of the functions, Fig. 5, and maps, Fig. 2, Fig. 3, Fig. 4, yielding from the numerical simulation of both temperature field and thermal gradient field. The method is able to reproduce / predict even the unique phenomenon of the SC - core appearance along the ingot axis, as well as formation of the $C+E$ – co-existence zone, Fig. 6.

The question arose whether both SC – core, and $C+E$ – zone could be predicted for copper rods manufactured under industrial condition in the Copper Smelter "Cedynia", until now, Fig. 7.

The adequate simulation was performed and both mentioned structure transitions: $C \Rightarrow C+E, C+E \Rightarrow E$, and $E \Rightarrow SC$, have been predicted by an adjustment of the gap between crystallizer and solidifying rod. In a response, such kind of the rod has been manufactured in the Copper Smelter "Cedynia", Fig. 8.
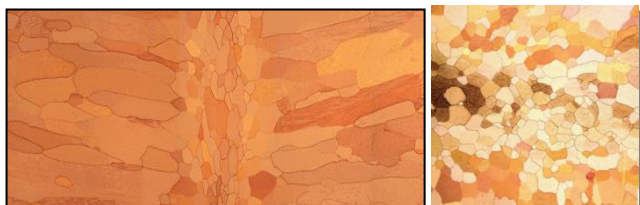

Fig. 7. Structure of the oxygen-free copper rod, a/ longitudinal section showing *structural zones*: C, $C+E$, and E, (no SC – core), b/ cross-section revealing a rod's area selected from the E – *structural zone*, only; (image, due to courtesy of the Copper Smelter "Cedynia" - KGHM Polska Miedź S.A.)

Fig. 8. Structure of the Cu-0.1Ag rod, a/ non-axial, longitudinal section showing *structural zones*: C, $C+E$, and E, b/ axial, longitudinal section revealing: $C+E$, E, and SC – *structural zones*; (image, due to courtesy of the Copper Smelter "Cedynia" - KGHM Polska Miedź S.A.)

In fact, the purposely manufactured rod presents the following *structural zones*: C, $C+E$, E, and the required SC - zone, Fig. 8.

7. Concluding remarks

A brief description of mathematical method for the prediction of the CET – localization in solidifying copper and copper alloys' ingots is presented. The method is to be preceded by numerical simulation of temperature and thermal gradient fields.

Some technological parameters like: heat transfer coefficient for solidification occurring inside the crystallizer, heat transfer coefficient for the secondary cooling system (air / ingot) and also others data, for example, relationships between heat transfer coefficient and gap size which are necessary in calculation are not delivered / revealed in the current model since the simulation itself is not a subject of considerations.

However, it should be noticed that the gap between the ingot and crystallizer has been considered as equal to 2.8 mm for the upper part of solidifying ingot and varies between $\delta = 0.0117$ mm, and $\delta = 0.0234$ mm for the lower part of ingot as it results from the converging inner surface of the crystallizer and the appearing ingot shrinkage.

The resultant functions and maps allow to follow the varying location of CET. Thus, it has been proven that the functions and maps are very sensitive on the thickness of the gap between solidifying ingot and crystallizer surface, Fig. 2.

The $CCFCT$ is marked schematically, Fig. 3, Fig. 6, and is connected with the cusp of the course of liquidus isotherm or thermal gradient in the proper map. More precise determination of the $CCFCT$ situation requires to determine the discontinuity of the first derivative of the algebraic function which could be used for the fitting of liquidus isotherm course.

The $FCCCT$ is marked schematically, Fig. 3a, Fig. 3b, and is connected with the point of inflection of the course of liquidus isotherm in the mentioned maps. More precise determination of the $FCCCT$ situation requires to determine the second derivative of the function which could be used for the fitting of liquidus isotherm course, Fig. 3a, Fig. 3b.

The CET is marked schematically, Fig. 3a, Fig. 3b, Fig. 4a, Fig. 4b, by the tangent to the point of maximum deviation of the liquidus isotherm course from its virtual linear course resulting from the extension imposed on the initial linear course. The method for determination of the deviation is shown schematically, Fig. 3a, Fig. 3b, Fig. 4a, Fig. 4b, and more detailly in Fig. 2.

The precise determination of CET localization requires to fit the course of the liquidus isotherm by an adequate algebraic function and find its maximum under investigation.

The CET localization is well confirmed schematically by the point of inflection visible in Fig. 3c, Fig. 4c. More precise determination of the point of inflection requires to calculate the second derivative of a function which could be used for fitting the liquidus isotherm course in Fig. 3c, Fig. 4c.

The liquidus isotherm velocity is drawn in function of the mushy zone length, Fig. 6. It was calculated for the corrected thickness of the gap a little lower than $\delta = 0.0234$ mm in order to create the possibility of the appearance of the single crystal core situated axially.

All the structural transitions like: $CC \Rightarrow FC$, $FC \Rightarrow C$, progressive $C \Rightarrow E$ accompanied by the $C+E$ zone existence, and sharp $E \Rightarrow SC$ are shown / determined schematically in Fig. 6. These transitions are not shown precisely because the current model makes attempt to describe the method which allows to distinguish *structure formation ranges* and resultant *structural zones* generally, only.

More precise determination of *structure formation ranges* and resultant *structural zones* requires to fit the liquidus isotherm velocity, Fig. 6, by an adequate algebraic function and to examine the behavior of its first, and second derivatives and possible discontinuity of the first derivative. It will allow to localize detailly the function extremum, point of inflection or function cusp if it appears.

The greater the gap thickness is imposed onto the system the minor volume fraction of the columnar structure can be expected. It can be justified by the position of maximum deviation of the liquidus isotherm from its virtual linear course, Fig. 2.

Consequently, the proportion index is lower when the gap thickness is greater. A significant effect of the crystallizer height on *CET* location is also expected.

Next, the effect of the pulling rate on the *CET* location has been studied, Fig. 3, Fig. 4. For the imposed pulling rate equal to: $u = 90$ cm/min. the columnar structure growth was completed at the ingot radius: $r \approx 0.05$ m, Fig. 3a, Fig. 3b.

When the pulling rate was equal to: $u = 250$ cm/min., then the columnar structure growth was completed at almost the same ingot radius: $r \approx 0.05$ m, Fig. 4a, Fig. 4b.

It is obvious that the pulling rate has not a substantial effect on the thickness of the columnar grains' shell in the ingot. The pulling rate more significantly results in time of *CET* appearance, which is equal to: $t \approx 5.3$ min. when $u = 90$ cm/min., Fig. 3b. *CET* appears at $t \approx 6.0$ min. when $u = 250$ cm/min., Fig. 4b. The effect of the pulling rate on *CET* situation is well visible while considering the distance from meniscus.

The distance $z \approx 0.48$ m, for $u = 90$ cm/min., Fig. 3a, and Fig. 3c, and $z \approx 1.5$ m, for $u = 250$ cm/min., Fig. 4a, and Fig. 4c.

Additionally, $CC \Rightarrow FC$, and $FC \Rightarrow C$ – sharp transitions were distinguished while considering maps generated from the numerical simulation performed for $u = 90$ cm/min.. Selection of the analogous structural transitions for $u = 250$ cm/min. requires to apply more discerning analyses of some features of the liquidus isotherm course located in maps being more precisely presented.

When some particular solidification conditions are imposed for the continuous casting then a unique phenomenon of the single crystal's core formation is observed, Fig. 5.

It can be explained through the rotation of the thermal gradient direction from its position parallel with columnar grains axis to its vertical direction, Fig. 5. The rotation occurs when a full heat accumulation is achieved in the solid shell. In this case, the casting system becomes adiabatic for heat output towards the crystallizer. It results in the appearance of the vertical heat flux. Strictly speaking, the system for continuous casting has been reduced to the *Bridgman's* system as required for single crystal growth accompanied with unidirectional heat transfer represented by the G_z - thermal gradient, Fig. 5.

Unusual phenomenon of the single crystal's core appearance has been subjected to control under the industrial condition in the Copper Smelter "Cedynia", Fig. 5b, Fig. 8, due to theoretical predictions for the $E \Rightarrow SC$ occurrence. The experience gained from the simulation resulting in the appearance of the $E \Rightarrow SC$ transition, Fig. 6, was helpful in performing the simulation of the temperature field and thermal gradient field adequate to the industrial condition as that applicable to the *Upcast* technology.

Finally, the gap thickness has been adjusted for such an industrial condition and applied in real process of the continuous casting in order to create the *SC - structural zone* in the Cu-0.1Ag rods produced in the Copper Smelter "Cedynia".

The structural confirmation of the single crystal core appearance is shown in Fig. 8. It is preceded by the analogous single crystal core formation in the Cu-0.1Ag strand, Fig. 5.

Thus, the applicability of the current mathematical method for the *structure formation ranges* has been confirmed in the industry.

The morphology shown in Fig. 5b, Fig. 8, provides an advantageous solution for the domestic economy. Rods of this type, subjected to plastic deformation, are used to manufacture overhead conductors for electric tractions whose high electric and heat conductivities are required. In this case, the created single crystal's core, Fig. 5b, Fig. 8b, improves the electric conductivity, whereas high fraction of the columnar structure, Fig. 5b, Fig. 8a, improves an efficient heat output into the ambiance.

A moderate fraction of the equiaxed structure which appeared with the presence of the co-existence zone of the $C+E$ structures within the rods manufactured in the Copper Smelter "Cedynia", Fig. 8, is sufficient for an easy plastic deformation essential in the overhead conductors' production, among others in the Power Cable Company, S.A. in Będzin.

The index defining a proportion between volume fractions of both considered types of the structure, $(C+SC)$ / E has been developed to control length of *structure formation ranges*, δ_i, along the mushy zone, taking into account interpretation of the liquidus isotherm velocity course as that shown in Fig. 6.

Acknowledgements

References

[1] Kurz, W., Fisher, D.J. (1998). Heat Extraction. In: *Fundamentals of Solidification* (pp. 5-19). Fourth Edition. CRC Press.

[2] McFadden, S., Browne, D.J., & Banaszek, J. (2006). Prediction of the formation of an equiaxed zone ahead of a columnar front in binary alloys castings: indirect and direct methods. *Materials Science Forum*. 508, 325-330. DOI:10.4028/www.scientific.net/MSF.508.325.

[3] Wołczyński, W. (2010). Constrained/unconstrained solidification within the massive cast steel/iron ingots.

Archives of Foundry Engineering. 10(2), 195-202. ISSN (1897-3310).

[4] Zimmermann, G., Sturz, L., Li, Y.Z., Nguyen-Thi, H., Mangelinck-Nöel, N., Fleurisson, R., Guillemot, G., Gandin, Ch.A., McFadden, S., Mooney, R.P., Voorhees, P., Roosz, A., Beckermann, C., Karma, A., Warnken, N., Perchat, E., Grün, G., Grohn, M., Poitrault, I., Toth, D. & Sillekens, W. (2018). Columnar and equiaxed solidification within the framework of the ESA MAP project CET-SOL. In the International Conference „Solidification and Gravity 2018", 3-6 September 2018 (pp. 17-26). Miskolc – Lillafüred, Hungary.

[5] Flood, S.C. & Hunt, J.D. (1998). Columnar to equiaxed transition. *Metals Handbook.* 15, 130-135.

[6] M'Hamdi, M., Bobadilla, M., Combeau, H., Lesoult, G. (1998). Numerical modeling of the columnar to equiaxed transition in continuous casting of steel. In Conference on Modelling of Casting, Welding and Solidification Processes VIII, 7-12 June 1998 (pp. 375-382). San Diego, California, USA.

[7] Dupouy, M.D., Camel, D., Mazille, J.E. & Hugon, I. (2000). Columnar to equiaxed transition in a refined Al-Cu alloy under diffusive and convective transport conditions. *Materials Science Forum.* 329-330, 25-30. https://doi.org/10.4028/www.scientific.net/MSF.329-330.25.

[8] Billia, B., Gandin, Ch. A., Zimmermann, G., Browne, D.J. & Dupouy, M.D. (2005). Columnar - equiaxed transition in solidification processes: the ESA-MAP CETSOL project. *Microgravity Science and Technology.* 16, 20-25. https://doi.org/10.1007/BF02945939.

[9] Yamazaki, M., Natsume, Y., Harada, H. & Ohsasa, K. (2006). Numerical simulation of solidification structure formation during continuous casting in Fe–0.7mass%C alloy using cellular automaton method. *The Iron and Steel Institute of Japan – International.* 46, 903-908. https://doi.org/10.2355/isijinternational.46.903.

[10] Gandin, Ch.A., Mosbah, S., Volkman, Th. & Herlach, D.M. (2008). Experimental and numerical modelling of equiaxed solidification in metallic alloys. *Acta Materialia.* 56(13), 3023-3035. DOI:10.1016/j.actamat.2008.02.041.

[11] Kumar, A. & Dutta, P. (2009). Numerical studies on columnar-to-equiaxed transition in directional solidification of binary alloys. *Journal of Material Science.* 44(15), 3952-3061. https://doi.org/10.1007/s10853-009-3539-z.

[12] Könözsy, L., Ishmurzin, A., Grasser, M., Wu, M., Ludwig, A., Tanzer, R. & Schützenhofer, W. (2010). Columnar to equiaxed transition during ingot casting using ternary alloy composition. *Materials Science Forum.* 649, 349-354. DOI:10.4028/www.scientific.net/MSF.649.349.

[13] Lorbiecka, A. & Šarler, B. (2010). A Sensitivity study of grain growth model for prediction of ECT and CET transformations in continuous casting of steel. *Materials Science Forum.* 649, 373-378. https://doi.org/10.4028/www.scientific.net/MSF.649.373.

[14] Mirihanage, W.U., Dai, H., Dong, H. & Browne, D.J. (2013). Computational modeling of columnar to equiaxed transition in alloy solidification. *Advanced Engineering Materials.* 15(4), 216-229. https://doi.org/10.1002/adem.201200220.

[15] Gandin, Ch.A., Billia, B., Zimmermann, G., Browne, D.J., Dupouy, M.D., Guillemot, G., Nguyen-Thi, H., Mangelinck-

Noël, N., Reinhart, G., Sturz, L., McFadden, S., Banaszek, J., Fautrelle, Y., Zaidat, K. & Ciobanas, A. (2006). Columnar-to-equiaxed transition in solidification processing (CET-SOL): a project of the European space agency (ESA) - microgravity applications promotion programme. *Materials Science Forum.* 508, 393-404. https://doi.org/10.4028/www.scientific.net/MSF.508.393.

[16] Noeppel, A., Budenkova, O., Zimmermann, G., Sturz, L., Mangelinck-Nöel, N., Jung, H., Nguyen-Thi, H., Billia, B., Gandin, Ch.A. & Fautrelle, Y. (2009). Numerical modeling of columnar to equiaxed transition – application to microgravity experiments. *International Journal of Cast Metals Research*, 22, 34-38. https://doi.org/10.1179/136404609X367272.

[17] Lemoisson, F., McFadden, S., Rebow, M., Browne, D.J., Froyen, L., Voss, D., Jarvis, D.J., Kartavykh, A., Rex, S., Herfs, W., Groethe, D., Lapin, J., Budenkova, O., Etay, J. & Fautrelle, Y. (2010). The development of a microgravity experiment involving columnar to equiaxed transition for solidification of a Ti-Al based alloy. *Materials Science Forum.* 649, 17-22. DOI:10.4028/www.scientific.net/MSF.649.17.

[18] McFadden, S., Browne, D.J., Sturz, L. & Zimmermann, G. (2010). Analysis of a microgravity solidification experiment for columnar to equiaxed transitions with modeling results. *Materials Science Forum.* 649, 361-366. https://doi.org/10.4028/www.scientific.net/MSF.649.361.

[19] Zimmermann, G., Sturz, L., Billia, B., Mangelinck-Nöel, N., Liu, D.R. Nguyen-Thi, H., Bergeon, N., Gandin, Ch.A., Browne, D.J., Beckermann, C., Tourret, D. & Karma, A. (2014). Columnar-to-equiaxed transition in solidification processing of AlSi7 alloys in microgravity - the CET-SOL project. *Materials Science Forum.* 790-791, 12-21. https://doi.org/10.4028/www.scientific.net/MSF.790-791.12.

[20] Huang, C., Hecht, U., Zollinger, J., Zaloznik, M., Viardin, A., Cisternas, M. (2018). Gravity dependent columnar-to-equiaxed transition in TiAl alloys: solidification of Ti-46Al-8Nb in hyper gravity and multi-physics modeling. In International Conference „Solidification and Gravity 2018", 3-6 September 2018 (pp. 42). Miskolc – Lillafüred, Hungary

[21] Wołczyński, W., Ivanova, A., Kwapisiński, P. & Olejnik, E. (2017). Structural transformations versus hard particles motion in the brass ingots. *Archives of Metallurgy and Materials.* 62(4), 2461-2467. DOI: 10.1515/amm-2017-0362.

[22] Kwapisiński, P., Lipnicki, Z., Ivanova, A. & Wołczyński, W. (2017). Role of the structural and thermal peclet numbers in the brass continuous casting. *Archives of Foundry Engineering.* 17(2), 49-54. DOI: 10.1515/afe-2017-0050.

[23] Wołczyński, W., Kwapisiński, P., Kania, B., Wajda, W., Skuza, W. & Bydałek, A.W. (2015). Numerical model for solidification zones' selection in the large ingots. *Archives of Foundry Engineering*, 15(4), 87-90. DOI: 10.1515/afe-2015-0085.

[24] Wołczyński, W., Ivanova, A., Kwapisiński, P. & Sztwiertnia, K. (2018). Effect of Pulling Rate on the Structural Zones' Localization in the Continuously Cast Brass Ingot. International Conference „Solidification and Gravity 2018", 3-6 September 2018 (pp. 131-137). Miskolc – Lillafüred, Hungary

[25] Szajnar, J. & Wróbel, T. (2008). Inoculation of pure aluminum aided by electromagnetic field. *Archives of Foundry Engineering*. 8(1), 123-132. ISSN (1897-3310).

[26] Rzadkosz, S., Kranc, M., Garbacz-Klempka, A., Piękoś, M. Kozana, J. & Cieślak, W. (2014). Research on technology of alloyed copper casting. *Archives of Foundry Engineering*. 14(2), 79-84. DOI:10.2478/afe-2014-0041.

[27] Piękoś, M., Garbacz-Klempka, A., Kozana, J. & Żak, P.L. (2020). Impact of Ti and Fe on the microstructure and properties of copper and copper alloys. *Archives of Foundry Engineering*. 20(4), 83-90. ISSN (2299-2944).